Journal of
Computational and Theoretical Nanoscience
Vol. 18, 1–10, 2021

Anomalous Conductance in Trans-Polyacetylene Chains with Even–Odd Parity

Jorsi J. da C. Cunha[1, 2], Miraci S. Costa[1], Antônio T. M. Beirão[3], Carlos A. B. da Silva Jr[4, *], Shirsley J. S. da Silva[4], and Jordan Del Nero[5]

[1] *Pós-graduação em Física, Universidade Federal do Pará, Belém-PA, 66075-110, Brazil*
[2] *Faculdade de Matemática, Universidade Federal do Pará, Breves-PA, 68800-000, Brazil*
[3] *Campus de Parauapebas, Universidade Federal Rural da Amazônia, Parauapebas-PA, 68515-000, Brazil*
[4] *Faculdade de Física, Universidade Federal do Pará, Ananindeua-PA, 67030-000, Brazil*
[5] *Faculdade de Física, Universidade Federal do Pará, Belém-PA, 66075-110, Brazil*

This work presents an analytical study of electronic transport in dimerized trans-polyacetylene (Trans PA) oligomers containing even ($n = 4$, 6, 8, 10 sites) and odd ($n = 3$, 5, 7, 9 sites) chains where the site C_1 is sandwiched by two metallic electrodes (*Left* and *Right*). These devices exhibit T-shaped geometry and are investigated by Su-Schrieffer-Heeger (SSH) model via Heisenberg equation of motion combined with the Keldysh formalism. We introduced disorder into the system through the dimerization force (δ) demonstrating that the dimerization in the chain can effectively lead to a linear (low δ) or zigzag (high δ) behavior, besides also suffering increase or decrease in conductance peak $[dI/dV]_{max}$. The odd chains exhibit trivial topological behavior to which the conductance peaks are suppressed as dimerization disorder is considered-creates barriers for tunneling. On the other hand, we have an opposite behavior for conductance peaks in the even chains. For example, the chain with weak dimerization (low δ) has a perfect transmission for even chains. In addition, we note for odd chains the formation of a plateau in the *I–V* curve for bias voltages and for even chains that show a linear current. This procedure shows an analytical study through the tunneling of the parameters on the device, such parameters as the tunneling amplitude ($\Gamma_{L/R}$) can be accessible experimentally.

Keywords: Conduct, Dimerization Correlations, Trans-PA, Electronic Transport, Keldysh Formalism.

RESEARCH ARTICLE

1. INTRODUCTION

Have been extensively investigated, low-dimensionality systems, such as conjugated polymers, allowing the study of essential aspects of quantum mechanics, structural properties, and transport in electronic devices [1, 2].

Typically, are defined carbon chains in the direction of electron transport, indicating a single path in the transmission process [3]. However, the graphene-type chain nanoribbon-1D + PA with T-shaped geometry suggest that the C_nH_n vertical chain can also actively participate in electron transmission, indicating that the transverse carbon chain is not the only way of transport on such devices [4].

In recent years, proposals for the realization of devices designed in the form of T-shaped received much attention from the scientific community, in particular working with the chain in zigzag connected to the *p*-type wave superconductor, allowing the detection of Majorana-bound states (MBS) [5, 6]. Xiong and Tong [7] proposed qubits of Majorana with mobilizable solitons combining the Su-Schrieffer-Heeger (SSH) model with "kitaev's toy model," inducing the superconducting phase by means of the proximity effect on the PA wire dimerized.

Motived by these investigations for T-shaped devices, we propose to study theoretically the electronic transport properties in finite-sized PA nanowires for chains even-odd type. Experimentally, the study of finite-length chains is relevant. Once, throughout the device, the semiconductor nanowire is considered segmented by disorder in a smaller number of coherent chains [8].

Electron transport decays exponentially due to the degree of disorder and the size of the chain [9]. In this

*Author to whom correspondence should be addressed.

paper, we analyze the electronic transport characteristics of a carbon chain:
(i) Controlled by the adjustment of different dimerization forces (δ), the parameter (δ) is the degree of the chain dimerization, the δ variation influences the transport properties electronic.
(ii) Dependence on the effects of the finite-length chain via curves for all bias windows. Due to the size of the chain, since as the disorder increases, it can lead to more localized states [10].

We obtain on the scale of nanodevices effects similar to those of microelectronics. At the level of nanodevice, circuit activation is obtained due to an external excitation in the structure of the SSH chain, like example, such as an external electric field or voltage and the photo stimulation corresponds to gate terminal [9].

Figure 1 shows the investigated T-shaped geometry system, composed of the trans-PA oligomer, covalently connected to two metallic electrodes (Left and Right). The coupling parameter (Γ) connect the electrodes to the first site (c_1) of the trans-PA oligomer. Is fixed the first site (c_1) at the other sites, forming the nanodevice in the geometry in the form of T-Shaped; the chain is dimerized by single $(1-\delta)$ and double $(1+\delta)$ bonds and is associated with the force of dimerization. Where $|\delta| < 1$ since 1 is the maximum tunneling for intra-site coupling and inter-site in the chain [11–13]. In the treatment of PA for the SSH model is introduced a simplification [14, 15] where only the *pi*-electrons responsible for the formation of the dimers, that is, only the normal mode of coupling vibration is considered, with that they are projected as ionic coordinates (displacement of the groups –CH) on the horizontal axis that extends through the geometer of the chain making the system one-dimensional. In short, the SSH model is an extension of the tight-binding approach. The experimental realization of the topology in one-dimensional systems (1D) [16, 17], made possible new and extensive investigations in the Su-Schrieffer-Hegger (SSH) model. The parameter that describes the tunneling or hopping dynamics is given by $(1-\delta)$ and $(1+\delta)$ along the chain in each unit cell in the 1D network in Figure 1, where δ is the dimerization force. The SSH model has as its main characteristic its two topologically different phases, which can be distinguished by the presence or absence, controlled by the adjustment of the dimerization intensity.

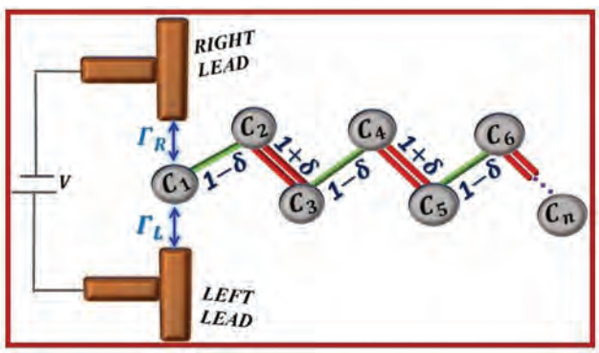

Fig. 1. Dimerized trans-PA oligomer with n sites whose site C_1 is coupled to two metallic electrodes (left lead and right lead) through the coupling parameter (Γ_L and Γ_R). The tunneling or hopping parameter is given by $(1-\delta)$ for single bond and $(1+\delta)$ for double bonding, where δ is the dimerization force. In our calculations, we consider the molecule with a number odd and even of sites.

We have adopted the analytical calculations the non-equilibrium Green's function (NEGF) [18, 19] for the system of Figure 1, in the Su-Schrieffer-Heeger (SSH) model [14]. Keldysh formalism is based on the Green's functions (retarded, advanced and minor) [20–23] and allows the treatment of interaction electrode-molecule-electrode in a self-consistently manner throughout the polarization range of interest applied [24, 25]. The devices exhibited good conductivity; can be found a robust oscillation effect in even chains.

The results for (i) adjustment of different dimerization forces (δ) and (ii) dependence on the effects finite length chain via *I–V* curves reveal that the intrinsic disorder obtained by the dimerization force (δ) is one of the most important parameters to capture the linear and non-linear tunneling in the consistent regime. This model can be distinguished through the presence or controlled absence of dimerization force. The effect of intrinsic disorder δt on the hopping force of the nearest neighbor through nanowire was investigated by Jun-Tong et al. [26] via NEGF of the tight-binding approach they focus on the properties of electronic transport, especially for zero polarization conductance peaks in the presence of disorder. In our article we studied intrinsic hopping disorder controlled specifically by δ (the dimerization force) described in the methodology, highlighting as an example $A = [1 + (-1)^n\delta]$ denotes the hopping between two adjacent unit cells for the even chain, we note that δ directly implies tunneling dynamics. That is, the intrinsic disorder parameters are controlled in our results by the numerical relationship between hopping and dimerization force.

In the next sections, we present the analytical calculation based on the NEGF and the "Results and discussions" section, we provide electronic transport results for different wire lengths and we discuss the different types of effect induced by dimerization in even and odd chains, respectively and in the last section we conclude.

2. METHODOLOGY

We considered a 1-D chain without spineless of the dimerized trans-PA oligomer whose site 1 (c_1) is coupled to metallic electrodes (left and right) by means of the symmetrical coupling factor Γ_L and Γ_R. The metallic electrodes used in the system are arbitrary and, if changed to gold, only will change the value of the chemical potential μ_L and μ_R [27, 28]. Equation (1) below shows the

RESEARCH ARTICLE

Hamiltonian of the system for a dimerized model with each carbon atom interacting with the nearest neighbor, is given by Equation (1)

$$H = H_L + H_{\mathrm{SSH}} + H_{\mathrm{LSSH}} \tag{1}$$

The first term H_L represents the Hamiltonian of the electrodes (left and right), which can be described by Eq. (2),

$$H_L = \sum_{k\alpha} \varepsilon_k c^{\dagger}_{k\alpha} c_{k\alpha} \tag{2}$$

where $c^{\dagger}_{k\alpha}\,(c_{k\alpha})$ denotes the electrons creation (annihilation) operators [29] in the electrodes [$\alpha =$ left (L) or right (R)]; ε_k represents the energy of the electrode at moment k.

The term H_{SSH} of the Eq. (1) describes a trans-PA molecule dimerized in the modified SSH model, to a chain containing n carbons, which can be written by Eq. (3),

$$H_{\mathrm{SSH}} = \sum_i \left\{ \left[1 + (-1)^i \delta \right] c^{\dagger}_i c_{i+1} + h \cdot c \right\} + h \sum_i c^{\dagger}_i c_i \tag{3}$$

where: $c^{\dagger}_i\,(c_i)$ creates (annihilates) electrons at site i. The chain index i, from 1 to n, is used to indicate the ith site of a 1-D the chain. The hopping between the nearest neighboring sites is staggered between $1+\delta$ and $1-\delta$ along the chain, so that each unit cell contains two sites, belonging to the two subsets generally indicated as A and B in *SSH* model [30]. Here we take the average of hopping integral as the unit of energy. The number 1 in hopping integrals (A and B) is the average of tunneling intensity. To ensure that the probability of displacement along the chain is equal, we considered $\delta < 1$. The parameter h represents the energy level [7].

The last term H_{LSSH} of the Eq. (1) describes the interaction between electrodes and the sites given by Eq. (4)

$$H_{\mathrm{LSSH}} = \sum_{k\alpha} V_{k\alpha} \left(c^{\dagger}_{k\alpha} c_1 + c^{\dagger}_1 c_{k\alpha} \right) \tag{4}$$

where $V_{k\alpha}$ is the electronic tunneling between the first site and the electrodes (left and right).

Using the recursive method of the *retarded Green's functions* for the first site $G^r_{c_1c_1}(\omega)$ that describe the configuration indicated in Figure 1 and based on the Heisenberg equation of motion we generalize the calculations to an even and odd number of n carbons contained in the chain of the dimerized trans-PA molecule.

In case, that n is even, we have the set of Eqs. (i)–(v)

$$(\omega - \varepsilon_k)\, G^r_{c_{k\alpha}c_1}(\omega) = V_{k\alpha} G^r_{c_1c_1}(\omega) \tag{i}$$
$$(\omega - h)\, G^r_{c_nc_1}(\omega) = B G^r_{c_{n-1}c_1}(\omega) \tag{ii}$$
$$(\omega - h)\, G^r_{c_{n-1}c_1}(\omega) = A G^r_{c_{n-2}c_1}(\omega) + B G^r_{c_nc_1}(\omega) \tag{iii}$$
$$(\omega - h)\, G^r_{c_{n-2}c_1}(\omega) = B G^r_{c_{n-3}c_1}(\omega) + A G^r_{c_{n-1}c_1}(\omega) \tag{iv}$$
$$\cdots$$
$$(\omega - h)\, G^r_{c_1c_1}(\omega) = 1 + B G^r_{c_2c_1}(\omega) + V_{k\alpha} G^r_{c_{k\alpha}c_1}(\omega) \tag{v}$$

where: (i) describes the dynamics of electrodes (Left and Right) through the Green's function and it's interaction with site 1; (ii) describes the interaction of site n with site $n-1$; (iii) describes the interaction of the site $n-1$ with the sites n and $n-2$, (iv) shows the interaction of the site $n-2$ with the sites $n-1$ and $n-3,\ldots$ (v) represents the dynamics of site *1* and it's interaction with electrodes (*Left* and *Right*) and site *2*. Replacing (ii) in (iii), (iii) in (iv), following this reasoning, we come to (v) and obtain the formula recursive of the Green's function retarded of site 1, with n sites, being n even, given by Eq. (5).

$$G^r_{c_1c_1}(\omega) = 1 \Big/ \omega - h - \frac{B^2}{\omega - h - (A^2/(\omega - h - \cdots - (B^2/\omega - h)))} + i\Gamma \tag{5}$$

where the hoppings $B = [1 + (-1)^{n-1}\delta]$ repeat $(n/2) - 1$ times and $A = [1 + (-1)^n \delta]$ repeat $n/2$ times.

For the case, which n is odd, we get the set of Eqs. (vi)–(x) similar to the set of Eqs. (i)–(v)

$$(\omega - \varepsilon_k)\, G^r_{c_{k\alpha}c_1}(\omega) = V_{k\alpha} G^r_{c_1c_1}(\omega) \tag{vi}$$
$$(\omega - h)\, G^r_{c_nc_1}(\omega) = A G^r_{c_{n-1}c_1}(\omega) \tag{vii}$$
$$(\omega - h)\, G^r_{c_{n-1}c_1}(\omega) = B G^r_{c_{n-2}c_1}(\omega) + A G^r_{c_nc_1}(\omega) \tag{viii}$$
$$(\omega - h)\, G^r_{c_{n-2}c_1}(\omega) = A G^r_{c_{n-3}c_1}(\omega) + B G^r_{c_{n-1}c_1}(\omega) \tag{ix}$$
$$\cdots$$
$$(\omega - h)\, G^r_{c_1c_1}(\omega) = 1 + B G^r_{c_2c_1}(\omega) + V_{k\alpha} G^r_{c_{k\alpha}c_1}(\omega) \tag{x}$$

The recursive formula of the *retarded Green's function* of site 1, for n sites, is given by Eq. (6), being n odd.

$$G^r_{c_1c_1}(\omega) = 1 \Big/ \omega - h - \frac{B^2}{\omega - h - (A^2/\omega - h - \cdots (A^2/\omega - h))} + i\Gamma \tag{6}$$

where the hoppings $A = [1 + (-1)^{n-1}\delta]$ and $B = [1 + (-1)^n \delta]$ repeat $(n-1)/2$ times.

The *retarded Green's function* of site 1, $G^r_{c_1c_1}(\omega)$ is important for our results, because we can of obtain the density of states (DOS) given by $\rho(\omega) = (-1/\pi)\, Im\left[G^r_{c_1c_1}(\omega)\right]$ whose results are present in Section 3.

In the Non-Equilibrium situation, we obtain the properties of electronic transport, such as the current and the differential conductance of the system versus the bias voltage through the NEGF, using the Keldysh formalism [18]. Is described the current by Eq. (7):

$$I_\alpha = 2eRe \left\{ \sum_{k\alpha} V_{k\alpha} G^<_{c_1k\alpha}(t, t') \right\} \tag{7}$$

where, $G^<_{c_1k\alpha}(t,t') = i\left\langle c^{\dagger}_{k\alpha}(t)\, , c_1(t') \right\rangle$ is the *minor Green's function*. Therefore, can be the current rewritten using the Landauer-Büttiker formula [31] given by Eq. (8):

$$I_{L/R} = \frac{2e}{h} \int T(E) \left[f_{L/R}(E) - f_{R/L}(E) \right] dE \tag{8}$$

where $T(E) = Tr\left[\Gamma^L G^r_{c_1} \Gamma^R G^a_{c_1}\right]$ is transmittance, $f_{L/R} = (1/e^{[(\varepsilon-\mu_{L/R})/k_BT]}+1)$ is the function of Fermi distribution in the chemical potential ($\mu_{L/R}$) in the electrodes and the $G^r_{c_1}(t,t') = -i\left\langle c_1(t), c_1^\dagger(t')\right\rangle$, $G^a_{c_1}(t,t') = i\left\langle c_1(t), c_1^\dagger(t')\right\rangle$ and $G^<_{c_1}(t,t') = i\left\langle c_1^\dagger(t), c_1(t')\right\rangle$ are the *Green's functions* (retarded, advanced and minor) for the site 1. As a departure point, via analytical continuation we get the *retarded Green's function* in the Keldysh contour $G_{c_1k\alpha}(\tau,\tau') = -i\left\langle T_c c(\tau), c^\dagger(\tau')\right\rangle$ where T_c the operators along the Keldysh contour. Let us now calculate the current. For a molecule of n sites, taking the temporal derivative of and $G^r_{c_1}(t,t')$, we obtain the Eq. (9)

$$\left(i\frac{\partial}{\partial t} - h\right) G^r_{c_1}(t,t') = \delta(t-t') + \sum_{k\alpha} V_{k\alpha} G^r_{c_1}(t,t') + BG^r_{c_{21}}(t,t') \tag{9}$$

With $G^r_{k\alpha}(t,t') = -i\left\langle T_c c_{k\alpha}(t), c_1^\dagger(t')\right\rangle$ and $G^r_{c_2}(t,t') = -i\left\langle T_c c_2(t), c_1^\dagger(t')\right\rangle$. Deriving $G^r_{k\alpha}(t,t')$ and $G^r_{c_2}(t,t')$ in t, we obtain the Eqs. (10) and (11),

$$\left(i\frac{\partial}{\partial t} - h\right) G^r_{c_{k\alpha}}(t,t') = V_{k\alpha} G^r_{c_1}(t,t') \tag{10}$$

$$\left(i\frac{\partial}{\partial t} - h\right) G^r_{c_2}(t,t') = BG^r_{c_1}(t,t') + AG^r_{c_3}(t,t') \tag{11}$$

where $G^r_{c_2}(t,t') = -i\left\langle T_c c_2(t), c_1^\dagger(t')\right\rangle$, which deriving in t we obtain Eq. (12),

$$\left(i\frac{\partial}{\partial t} - h\right) G^r_{c_3}(t,t') = AG^r_{c_2}(t,t') + BG^r_{c_4}(t,t') \tag{12}$$

Continuing in the same way, we arrive at Eq. (13),

$$\left(i\frac{\partial}{\partial t} - h\right) G^r_{c_n}(t,t') = AG^r_{c_{n-1}}(t,t') \tag{13}$$

The Eqs. (9)–(13) constitute a complete set of $n+1$ differential equations that describe the interactions between electrodes with the first site (c_1) and between the neighboring sites (c_n), see Figure 1. May be written the Eq. (10) in integral form, given by Eq. (14),

$$G^r_{k\alpha}(t,t') = \int dt_1 g^r_{n,k\alpha}(t,t_1) V_{k\alpha} G^r_{c_1}(t,t') \tag{14}$$

where, $g^r_{n\cdot k\alpha}(t,t_1) = -i\left\langle T_c c_{k\alpha}(t), c_1^\dagger(t_1)\right\rangle$. Replacing Eqs. (14) in (9), we obtain the Eq. (15),

$$\left(i\frac{\partial}{\partial t} - h\right) G^r_{c_1}(t,t') = \delta(t-t') + \int dt_1 \sum_{(t,t_1)} G^r_{c_1}(t,t') + BG^r_{c_2}(t,t') \tag{15}$$

with $\sum_{(t,t_1)} = \sum_{k\alpha} g^r_{k\alpha}(t,t_1)|V_{k\alpha}|^2$. Therefore, we reduced the system of n differential equations, which can be written in integral form. In a matrix notation, they are given by Eq. (16),

$$\vec{G}(t,t') = g(t,t')\vec{u} + \iint dt_2 dt_1 g(t,t_2) \times \sum{}'(t_2,t_1)\vec{G}(t_1,t') \tag{16}$$

where $\vec{u}$ is the unitary vector. Using Eq. (16), we get the Dyson Equation for the system,

$$G(t,t') = g(t,t') + \iint dt_2 dt_1 g(t,t_1) \sum{}'(t_1,t_2) G(t_2,t') \tag{17}$$

Due to the convolution-time integrals in the above equations, it is useful to make Fourier transforms of the *Green's functions*. Therefore, in the Keldysh contour [30] we have Eq. (18),

$$G(\tau,\tau') = g(\tau,\tau') + \iint d\tau_2 d\tau_1 g(\tau,\tau_1) \tilde{\sum}(\tau_1,\tau_2) G(\tau_2,\tau') \tag{18}$$

Next, we apply Langreth's analytic continuation in Eq. (18), we get the *retarded Green's function* by Eq. (19),

$$G^r(\omega) = g^r(\omega) + g^r(\omega) \tilde{\sum}^r(\omega) G^r(\omega) \tag{19}$$

In addition, for the minor Green's function, we have the Eq. (20),

$$G^<(\omega) = G^r(\omega) \tilde{\sum}^<(\omega) G^a(\omega) \tag{20}$$

The equations obtained for the *retarded/advanced/minor Green's functions* form a set of integral-dependent equations and a set of matrix equations in the energy representation. Note that all of the above equations for the three real-time *Green's functions* are exact and general in the meaning of the perturbation expansion, that is, when one can define self-energies [32].

From where we get the components of retarded and minor self-energy given by the following matrix,

$$\tilde{\sum}^r_{11}(\omega) = \begin{bmatrix} -\frac{i}{2}\Gamma(\omega) & B & 0 & 0 & & \\ & 0 & A & 0 & 0 & \\ B & & A & 0 & B & 0 \\ 0 & & 0 & B & 0 & 0 \\ 0 & & \cdots & \cdots & \cdots & \cdots \\ \cdots & & 0 & 0 & 0 & 0 \\ 0 & & & & & \end{bmatrix} \tag{21}$$

and the matrix $\tilde{\sum}^<(\omega)$ has a nonzero element in Eq. (21),

$$\tilde{\sum}^r_{11}(\omega) = i\left[\Gamma_L(\omega) f_L(\omega) + \Gamma_R(\omega) f_R(\omega)\right] \tag{22}$$

Self-energies are complex Green's functions and have interesting physical meaning, the real part causes a change in its own values, while the imaginary part is responsible lifetime in the electronic state, this process produces an enlargement of Density of States (DOS). Therefore, with the Eqs. (19) and (20) we can calculate the current of the system.

3. NUMERICAL RESULTS

Initially, we developed calculations at the thermodynamic limit in the context of the Green's functions [33, 34] for the metal/trans-PA/metal system (corresponding to odd–even sites), and assuming $\Gamma_{L/R} = 0.5$ eV between the molecular level and the electrodes. The control for the free parameters used are $h = 0$ eV to adjust the only accessible energy level on the site (c_1) Fermi level $\omega = 0$ eV. The parameter δ represents the adjustable dimerization force. For obtain better tunneling, we consider $0 < \delta < 1$ to ensure equality in the probability of displacement along the chain and ensure best results when δ values are near to zero, as show in Figure 4(a) in the paper for $\delta = 0.01$ eV that confirms an almost perfect conduction. The model will regress to the Kitaev's model when $\delta = 0$ eV and the molecule becomes a polyne-type carbyne when $\delta = 1$ eV, once 1 allows maximum tunneling for intrasite-to-intersite coupling in the chain [11–13].

Figure 2(a) exhibits Density of States (DOS) at $V = 0$ V for odd chains ($n = 3, 5, 7, 9$). The DOS strong and broad peaks appear at the Fermi level for dimerization force $\delta =$ 0.1 eV while the Figure 2(b) for the even chains ($n =$ 4, 6, 8, 10) exhibit the peaks in DOS situated (*gap* to the finite size) at the Fermi level that contribute to the emergence of more transmission channels than the odd chain. An efficient coupling in T-shaped shape can be found on the device, DOS displays well-matched channels for electrons contribute to transmittance in nanodevice.

Figures 2(c) and (d) present the energy-dependent transmittance [*T(E)*] for odd and even chains, respectively. Figure 2(c) shows that the transmittance is greater for short chains. The transmittance in even chains, see Figure 2(d), is greater than for odd chains because it has a greater contribution, as accessible multichannel emerge and approach the Fermi level. The DOS and *T(E)* depend on odd-even parity, where we observe a clear difference between odd and even chains; Jing-Xin et al. [35] predicted this

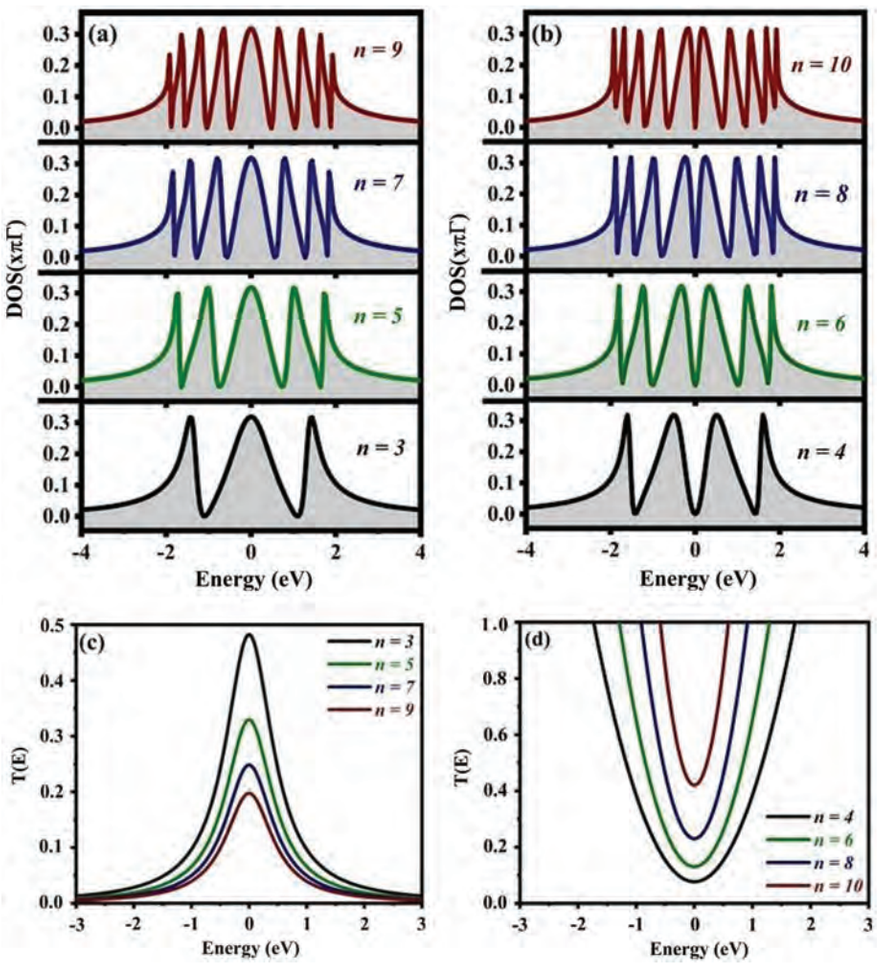

Fig. 2. DOS and Transmittance [T(E)] versus Energy for the metal/trans-PA/metal system with symmetrical coupling $\Gamma_{L/R} = 0.5$ eV; hoppings between neighboring sites, $A = 1 + \delta$ and $B = 1 - \delta$ where $\delta = 0.1$ eV and energy level, h = 0.0 eV. (a) DOS for odds chains, (b) DOS for even chains, (c) *T(E)* for odds chains and (b) *T(E)* for even chains.

behavior. It is observed that the transmission probability is characterized by the presence of peaks at 0.0 eV. Figure 2(c) shows; (1) a qualitative transmission signature for the odd number of sites, but (2) for the case of the even-local dimer chain at 0.0 eV energy, a decrease the transmission probability with increasing length of the chain, the Figure 2(d) show probability that an electron is reflected from in even chain.

In Figure 3(a), it is exhibited the characteristics of the electronic transport by *I–V* curves, for the parameters $\Gamma_{L/R} = 0.5$ eV and $\delta = 0.1$ eV for odd chains $3 \leq n \leq 17$ sites. In the linear response regime indicated by 0.0 V $\leq$ V $\leq$ 0.5 V inserted in the Figure 3(a), the current has a finite slope. As the bias voltage increases above linear response regime 0.6 V $\leq$ V $\leq$ 2.0 V, it is observed that the current profile presents a single plateau at 2.0 V, *I–V* curve tends to a saturation region. In Figure 3(b) the differential conductance ($G = dI dV$) features the standard Lorentzian with broadening given by $\Gamma = \Gamma_L + \Gamma_R$ with almost invariant pattern for polarization voltage up to 0.5 V (insert in Fig. 3(b)).

In Figure 4(a), it is investigated the effect of tunneling, through different dimerization force (δ) controlling the electronic tunneling for five sites (i.e., $n = 5$). The dimerization force (δ) in the hopping $A = 1 + \delta$ (double bond)

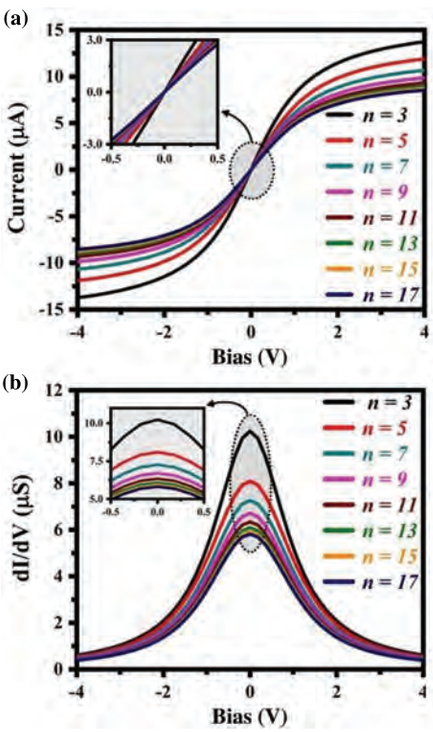

Fig. 3. Electronic transport to odd chains ($n = 3$, 5, 7, 9, 11, 13, 15 and 17 sites) coupled to electrodes (Left and Right) with parameters, $\Gamma_{L/R} = 0.5$ eV and $\delta = 0.1$ eV: (a) *I–V* curve with voltage from −4 V to 4 V. In the inset (a), we have current for low bias voltage and (b) $dI/dV - V$ curve, highlighting the resonance peaks at insert (b).

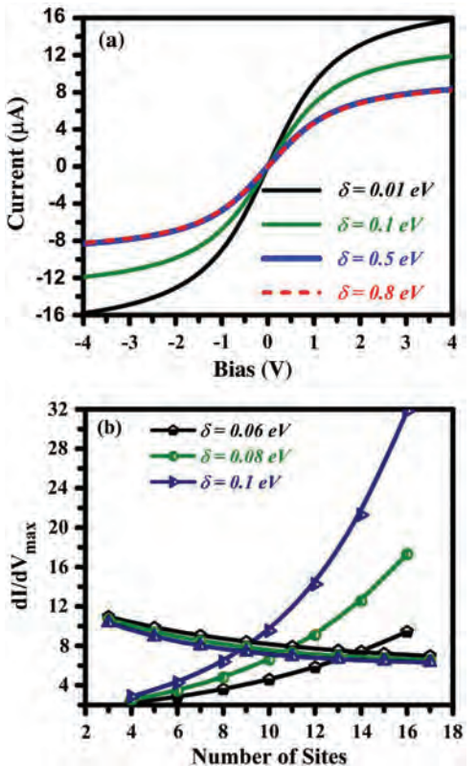

Fig. 4. (a) *I–V* curve for the chain with five sites $n = 5$ considering four different values for the parameter δ: (1) 0.01 eV; (2) 0.1 eV; (3) 0.5 eV; and (4) 0.8 eV, keeping $\Gamma_{L/R} = 0.5$ eV. (b) The maximum conductance for chain with even and odd sites keeping $\Gamma_{L/R} = 0.5$ eV and varying δ, i.e., 0.06 eV, 0.08 eV and 0.1 eV.

and $B = 1 - \delta$ (single bond), respectively is adopted as: $\delta = 0.01$ eV; $\delta = 0.1$ eV; $\delta = 0.5$ eV and/or $\delta = 0.8$ eV. It is observed that the *I–V* curve for $\delta = 0.01$ eV (black curve) and $\delta = 0.1$ eV (blue curve) shows an almost perfect drive, that is, an almost flat chain ($\delta = 0.0$ eV). However, for the chain dimerized with $\delta = 0.5$ eV (red curve) and $\delta = 0.8$ eV (green curve) the tunneling is smaller and approximately equal to $\delta = 0.6$ eV. This condition can be interpreted as structural and conformational defects that reduce the overlapping states, acting as locator centers that interrupt conjugation along the polymer chain.

Figure 4(b) exhibits the maximum conductance $[dI/dV]_{\max}$ depending on the number of sites and dimerization force $\delta = 0.06$ eV; $\delta = 0.08$ eV and $\delta = 0.1$ eV. For odd chains ($n = 3, 5, 7, 9, 11, 13, 15$ and 17 sites), there is a decrease in maximum conductance related to the increase in the chain (n) and dimerization force (δ) that vary approximately between 11 μA/V and 5 μA/V confirmed in the *I–V* curve, as can seen in Figure 4(a). Also in Figure 4(b), it is examined $[dI/dV]_{\max}$ for the even chains ($n = 4$, 6, 8 and 10 sites), a behavior clearly different from those obtained for the odd chains. For example, the supply chain dimmers with $\delta = 0.1$ eV has a perfect conduction. In this case, the increase in dimerization strength

RESEARCH ARTICLE

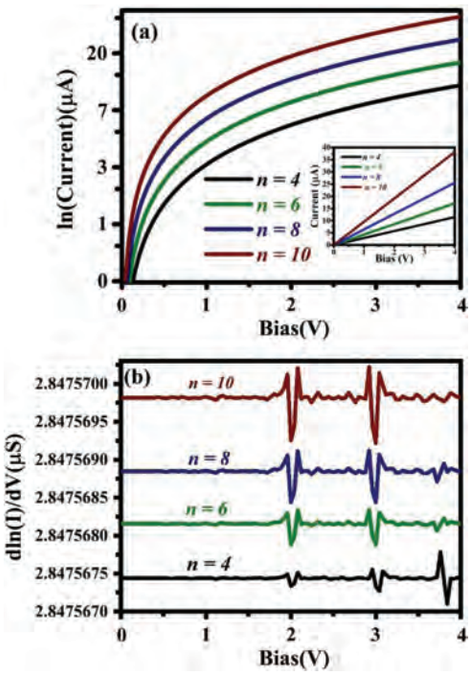

Fig. 5. (a) $\ln(I)$–V curve and (b) $dln(I)/dV$ curve for even chains (4, 6, 8 and 10 sites) with the parameters $\Gamma_{L/R} = 0.5$ eV and $\delta = 0.1$ eV. The insert in (a) shows the I–V curves for these chains.

contributes to the creation of states localized at the Fermi level. It can be confirm this characteristic in the DOS plot, see Figure 2(b). As a result, can be transferred the electron coherently from one state of energy to another, since these relocated states are close to the Fermi level and are sensitive to the entire uniform chain.

Now, it is done the analyze for the electronic transport in the even chains (i.e., $n = 4, 6, 8$ and 10) for a dimerization force $\delta = 0.1$ eV in according with the Figure 4(b), as it provides a additional information to describe the influence of disorder on the system.

In Figure 5(a) for even chains (i.e., $n = 4, 6, 8$ and 10), the $\ln(I)$–V curve displays a quasi-ohmic region up to 0.5 eV. Then the current it increases very slowly, and the slope is due to the different resistances offered. Figure 5(b) shows that conductance peaks are due to the gradual increase in excitation states available in the pair chain as tunneling paths. These oscillations allow us to obtain information about the dynamics of carriers. This effect was experimentally confirmed for the Au, Pt and Ir wires through the by means mechanically controllable break junctions (MCBJ) [36]. Lang and Avouris [37] showed that at the low voltage limit the oscillations for even chains are greater than for odd chains and then Larade et al. [38] extended their investigation to higher finite voltages and found a similar result. Such effects are attributed to charge transfer in different paths involving hopping between adjacent sites A and B in the same cell or not due to different topologies chain order [35].

Now, it is exhibited the DOS and $T(E)$ for a strong dimerization $\delta = 0.6$ eV of the even chain. Figure 6(a) exhibits states located near at the Fermi level while Figure 6(b) has a wide and tilting window of the tail, where the Fermi level is close to the driving band region [38]. Figure 6(b) has a wide transmission window displaying a greater contribution to long chains. The insertion of Figure 6(b) shows the range of $n = 4, 6$ and 8 for small transmissions.

Figure 7(a) exhibits the I–V curve for dimerization $\delta = 0.6$ eV. The current increases to $V = 1.2$ V and saturates the electronic transport affected by oscillations at $V > 1.2$ V. For oscillations intermediate, $\delta = 0.6$ eV depend on the states localized and delocalized. In Figure 7(b) for $\delta = 0.6$ eV, the peaks in concordance are oscillations and show the appearance of barriers. The chain of dimer for $\delta = 0.6$ eV indicates that, as the disorder increases, the states became more localized.

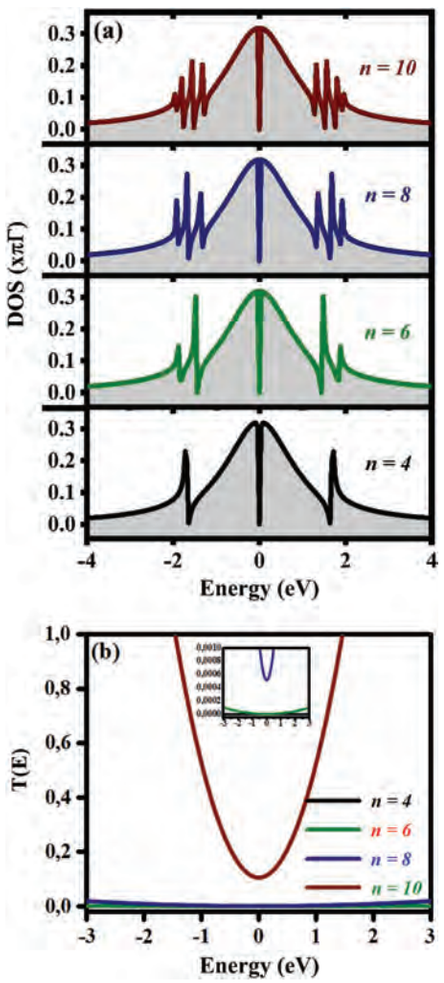

Fig. 6. (a) DOS and (b) transmittance $T(E)$ with symmetric coupling $\Gamma_{L/R} = 0.5$ eV and $\delta = 0.6$ eV, for even chains (4, 6, 8 and 10 sites). In (b) an insert shows the $T(E)$ behavior for 4, 6 and 8 sites.

RESEARCH ARTICLE

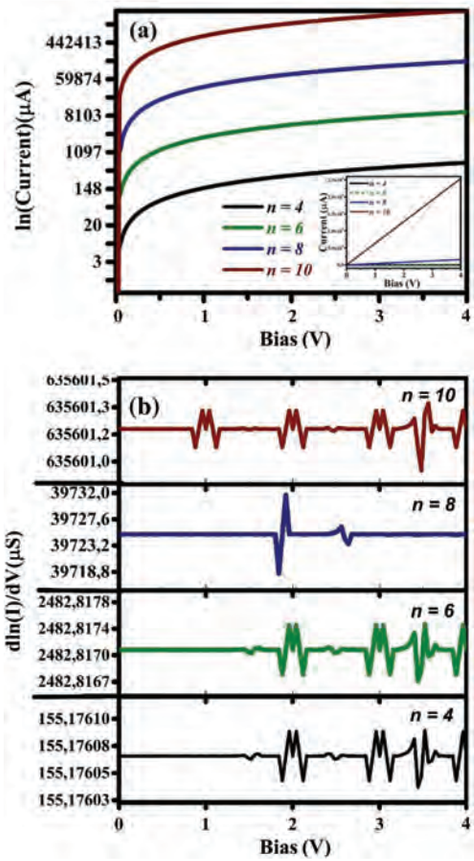

Fig. 7. (a) $\ln(I)$–V curve and (b) $dln(I)/dV$ for 4, 6, 8 and 10 sites, with the parameters $\Gamma_{L/R} = 0.5$ eV and $\delta = 0.6$ eV. The insert in (a) shows the I–V curves.

In summary, for $\delta = 0.1$ eV in the odd chain (i.e., $n = 3$, 5, 7 and 9 sites), the system has a metallic behavior until 0.5 V going from metal to semiconductor between $0.6\ \text{V} \leq \text{V} \leq 2.0$ V. For even chains (i.e., $n = 4$, 6, 8 and 10 sites) we have: (i) for $\delta = 0.1$ eV, the increase in the I–V curve; (ii) to $\delta = 0.6$ eV, undergoes an increased oscillations in the conductance curves. Transitions in electrical behavior of Molecular Devices [39] were recently investigated. In this paper for zero polarization 0.0 V, the odd chains have a metallic behavior, see DOS in Figure 2(a). However, when the voltage increases the current grows up to 0.5 V where quasi-uniform up to 0.6 V which is the beginning of the resonance and then grows up to with a linear growth for greater polarization. The resonance points confirm the occurrence of a change in the I–V curve and the electronic transition.

On the other hand, the Figure 2(b) shows the even chains for $\delta = 0.1$ eV, where the DOS at 0.0 V exhibits contributions of the delocalized peaks in the entire energy range. Also in Figure 2(b) the DOS at 0.0 V shows peaks and gaps near the Fermi level (ε_F) with Energy gap < 0.1. Still for even chains, Figure 6(b) for $\delta = 0.6$ eV there are clear peaks around ε_F show gap $\ll 0.1$ eV, this is visible in Figure 7(a), still in Figure 6(b) for the 2.0 eV range, DOS shows the states located. The I–V curve in the Figure 7(a) does not identify the small characteristic oscillations, since the transport is done via direct tunneling through the barrier model (the graph is a straight line as the tension is increased). However, the graph of differential conductance $G = dI/dV$ in Figure 7(b) shows oscillations, that is $G = dI/dV$ is sensitive to the presence of localized states from the range of 2.0 eV visible in the DOS of Figure 6(b).

The results obtained through analytical calculations show peculiar differences between odd-even parity chains in the T-shaped device, due to the topology of the chain.

4. CONCLUSION

We investigated the effect of intrinsic disorder the transport properties of polyacetylene of even-odd chain, adopting the Keldysh's formalism. We introduce disorder into the system as dimerization forces (δ): strong type $\delta = 0.1$ eV, $\delta = 0.5$ eV, $\delta = 0.6$ eV and weak type $\delta = 0.01$ eV, $\delta = 0.06$ eV and $\delta = 0.08$ eV. For odd chain, the presence of disorder is controlled to $\delta = 0.1$ eV (low dimerization) which allows an exponential increase in the I–V curve and a pronounced peak in conductance see Figures 3(a) and (b). Therefore, for high bias voltage, starting at 2.0 V, the conductance spectra decrease monotonically and electronic signature is the predominant voltage function applied in the system. On the other hand, for the even chain with $\delta = 0.1$ eV it reduces the location of the conductance around 0.0 eV and for $\delta = 0.6$ eV for even chain, localized states arise, leading to an increase in the division of the peaks. This is seen in Figure 4(b) due to the higher conductance for the even chain indicating an electronic signature with greater influence of the dimerization force parameter of the even chain.

We demonstrate that the disorder can displace the peak in the differential conductance. The odd chain exhibits trivial topological behavior that we can see it in the transmission electronic of the system for odd chain; the magnitude of the conductance peaks is considerably suppressed as the disorder is taken into account.

On the other hand, we have an opposite behavior in the pair chain, seen in Figure 4(b). For example, the dimer chain with $\delta = 0.06$ eV strong has an almost perfect transmission. We can be attributing this behavior to the appearance of DOS. This corroborates the dynamic of electrons in the device, via electronic tuning and the topologic of the system. This procedure shows an analytical and numerical study in with experimentally accessible parameters. Therefore, it can be applied to systems such as Condensed Matter/Cold Atom [40, 41], which were proposed as semiconductor wires with states located through a defect in the chain. It has already been verified that some physical systems, for example, the two-dimensional graphene tape [42] and the p-orbital optical lattice [46], can be mapped to the SSH model. Such devices have applications as in qubits

with mobilizable solitons in an extended SSH model qubit in quantum computer application [7]. The present model investigated through the control of intrinsic parameters allows the system to behave like a molecular structure like carbine and even the kitaev's chain model [5] for topological formation of protected states as observed in photonic quantum walks [44].

Acknowledgments: The authors thank to Brazilian funding agencies PROPESP/UFPA–PIBIC Interior-project PRO2653-2018 and CNPq (Conselho Nacional de Desenvolvimento Científico e Tecnológico)-project CNPq/306266/2017-2. J.C.C. thanks to PPGF and Júlio César Santos.

References

1. Aleixo, V.F.P., Silva, C.A.B. and Del Nero, J., **2014**. Molecular electronic junction composed by C60 as spacer and four terminals formed by acceptors group: Transition-voltage spectroscopy. *Journal of Computational and Theoretical Nanoscience, 11*(3), pp.1–5.
2. McCreery, R.L., **2004**. Molecular electronic junctions. *Chemistry of Materials, 16*(23), pp.4477–4496.
3. Jayasekera, T. and Mintmire, J.W., **2007**. Transport in multiterminal graphene nanodevices. *Nanotechnology, 18*(42), p.424033.
4. He, J.J., Yan, X.D., Guo, C.S., Liu, Y.D., Xiao, Y. and Meng, L., **2016**. The electron transport properties of zigzag graphene nanoribbons with upright standing linear carbon chains. *Solid State Communications, 227*, pp.28–32.
5. Beirão, A.T.M., Costa, M.S., Oliveira, A.S., Cunha, J.J.C., da Silva, S.S. and Del Nero, J., **2018**. Majorana bound states in a quantum dot device coupled with a superconductor zigzag chain. *Journal of Computational Electronics, 17*(3), pp.959–966.
6. Bühler, A., Lang, N., Kraus, C.V., Möller, G., Huber, S.D. and Büchler, H.P., **2014**. Majorana modes and p-wave superfluids for fermionic atoms in optical lattices. *Nature Communications, 5*(1), p.4504.
7. Xiong, Y. and Tong, P.A., **2015**. NOT operation on Majorana qubits with mobilizable solitons in an extended Su-Schrieffer-Heeger model. *New Journal of Physics, 17*(1), p.013017.
8. Mouruk, V., Zuo, K., Frolov, S.M., Plissard, S.R., Bakkers, E.P.A.M. and Kouwernhoven, L.P., **2012**. Signatures of majorana fermions in hybrid superconductor-semiconductor nanowire devices. *Science, 336*, pp.1003–1007.
9. Oliveira, A.S., Beirão, A.T.M., Silva, S.J.S. and Del Nero, J., **2018**. Electronic signature of single-molecular device based on polyacetylene derivative. *Journal of Computational Electronics, 17*(2), pp.586–594.
10. Anderson, P.W., **1985**. The question of classical localization a theory of white paint? *Philosophical Magazine B, 52*(3), pp.505–509.
11. Saitner, M., Eberle, F., Baccus, J., D'Olieslaeger, M., Wagner, P., Kolb, D.M. and Boyen, H.G., **2012**. Impact of functional groups onto the electronic structure of metal electrodes in molecular junctions. *The Journal of Physical Chemistry C, 116*(41), pp.21810–21815.
12. Wei, J.H., Liu, X.J., Xie, S.J. and Yan, Y., **2009**. Spin-dependent current modulation in organic spintronics. *The Journal Chemical Physics, 131*(6), p.0649061.
13. Nakayama, H. and Kimura, S., **2011**. Oligo(phenyleneethynylene) as a molecular lead for STM measurement of single molecule conductance of a helical peptide. *Chemical Physics Letters, 508*(4–6), pp.281–284.
14. Su, W.P., Schrieffer, J.R. and Heeger, A.J., **1980**. Soliton excitations in polyacetylene. *Physical Review B, 22*(4), pp.2099–2111.
15. Su, W.P., Schrieffer, J.R. and Heeger, A.J., **1979**. Soliton in polyacetylene. *Physical Review Letters, 42*(25), pp.1698–1701.
16. Thouless, D.J., Kohmoto, M., Nightingale, M.P. and den Nijs, M., **1982**. Quantized Hall conductance in a two-dimensional periodic potential. *Physical Review Letters, 49*(6), pp.405–408.
17. Xiao, M., Ma, G., Yang, Zh., Sheng, P. and Zhang, Z.Q., **2015**. Role of transparency of platinum-ferromagnet interfaces in determining the intrinsic magnitude of the spin Hall effect. *Nature Physics, 11*(6), pp.496–502.
18. Keldysh, L.V., et al., **1965**. Diagram technique for nonequilibrium processes. *Soviet Physics-JETP, 20*(4), pp.1018–1026.
19. Saifi, H. and Ahsan, M.A.H., **2014**. Electron transport in T-shaped double quantum Dor system using non-equilibrium Green's function. *Journal of Computational and Theoretical Nanoscience, 20*(7), pp.1281–1286.
20. Galperin, M., Ratner, M.A. and Nitzan, A., **2007**. Molecular transport junctions: Vibrational effects. *Journal of Physics Condensed Matter, 19*(10), p.103201.
21. Koch, T., Loos, J., Alvermann, A. and Fehske, H., **2011**. Nonequilibrium transport through molecular junctions in the quantum regime. *Physical Review B, 84*(12), p.125131.
22. Koch, T., Fehske, H. and Loos, J., **2012**. Phonon-affected steady-state transport through molecular quantum dots. *Physica Scripta, 2012*(T151), pp.014039.
23. Costa, M.S., Beirão, A.T.M., da Silva, C.A.B., da Silva, S.J.S., Nero, J.D., **2020**. Majorana field effect transistor. Majorana fermion detection and transport properties. *Journal of Computational and Theoretical Nanoscience, 17*(11), pp.4826–4834.
24. Wei, J.H., Xie, S.J., Mei, L.M., Berakdar, J. and Yan, Y., **2005**. Charge-transfer polaron induced negative differential resistance and giant magnetoresistance in organic spin-valve systems. *New Journal of Physics, 8*(5), p.82.
25. Wei, J.H., Xie, S.J., Mei, L.M., Berakdar, J. and Yan, Y., **2007**. Conductance switching, hysteresis, and magnetoresistance in organic semiconductors. *Organic Electronics, 8*(5), pp.487–497.
26. Jun-Tong, R., Hai-Feng, L., Sha-Sha, K., Yong, G. and Huai-Wu, Z., **2018**. Disorder-induced suppression of the zero-bias conductance peak splitting in topological superconducting nanowires. *Beilstein Journal of Nanotechnology, 9*(1), pp.1358–1369.
27. Braun, S., Salaneck, W.R. and Fahlman, M., **2009**. Energy-level alignment at organic/metal and organic/organic interfaces. *Advanced Materials, 21*(14–15), pp.1450–1472.
28. Malen, J.A., Yee, S.K., Majundar, A. and Segalman, R.A., **2010**. Fundamentals of energy transport, energy conversion, and thermal properties in organic–inorganic heterojunctions. *Chemical Physicis Letters, 491*(4–6), pp.109–122.
29. Bruus, H. and Flensberg, K., **2006**. *Many-Body Quantum Theory in Condensed Matter Physics*. New York, USA, Oxford University Press. p.466.
30. Shen, S.Q., **2012**. *Topological Insulators, Dirac Equation in Condensed Matters*. Springer Series in Solid-State Science, Berlin, Germany, Vol. 174, p.225.
31. Haug, H. and Jauho, A.P.S. ed., **2008**. Quantum Kinetics in Transport and Optics of Semiconductors. *Springer Series in Solid-State Sciences*, Vol. 123, p.339.
32. Do, V.N., **2014**. Non-equilibrium Green function method: Theory and application in simulation of nanometer electronic devices. *Advances in Natural Sciences: Nanoscience and Nanotechnology, 5*(3), p.033001.
33. Kraus, C.V., Diehl, S., Zoller, P. and Baranov, M.A., **2012**. Preparing and probing atomic Majorana fermions and topological order in optical lattices. *New Journal of Physics, 14*(11), p.113036.
34. Law, K.T., Lee, P.A. and Ng, T.K., **2009**. Majorana fermion induced resonant Andreev reflection. *Physical Review Letters, 103*(23), p.237001.

RESEARCH ARTICLE

35. Jing-Xin, Y., Zhi-Wei, H. and Xiu-Ying, L., **2015**. Stability of conductance oscillations in carbon atomic chains. *Chinese Physics B, 24*(6), p.067307.
36. Wang, L., Ling, W., Zhang, L. and Xiang, D., **2017**. Advance of mechanically controllable break junction for molecular electronics. *Topics in Current Chemistry, 375*(61), pp.61–68.
37. Lang, N.D. and Avouris, P.H., **1998**. Oscillatory conductance of carbon-atom wires. *Physical Review Letters, 81*(16), pp.3515–3518.
38. Larade, B., Taylor, J., Mehrez, H. and Guo, H., **2001**. Conductance, $I-V$ curves, and negative differential resistance of carbon atomic wires. *Physical Review B, 64*(7), p.075420.
39. dos Santos, J. C., da, S., Ferreira, D.F.S., da Silva Jr., C.A.B. and Del Nero, J., **2020**. Transitions in electrical behavior of molecular devices based on 1-D and 2-D graphene-phagraphene-graphene hybrid heterojunctions. *Materials Chemistry Physics, 253*, p.123420.
40. Jiang, L., et al., **2011**. Majorana fermions in equilibrium and in driven cold-atom quantum wires. *Physical Review Letters, 106*(22), p.200402.
41. Zhang, C., Tewari, S., Lutchyn, R.M. and Sarma, S., **2008**. px+ ipy Superfluid from s-wave interactions of Fermionic cold atoms. *Physical Review Letters, 101*(16), p.160401.
42. Ryu, S. and Hatsugai, Y., **2002**. Topological origin of zero-energy edge states in particle-hole symmetric systems, *Physical Review Letters, 89*(7), p.077002.
43. Bloch, I., **2008**. Quantum coherence and entanglement with ultracold atoms in optical lattices. *Nature, 453*, p.7198.
44. Cardano, F., et al., **2016**. Statistical moments of quantum-walk dynamics reveal topological quantum transitions. *Nature Communications, 7*(1), p.11439.

Received: 31 March 2021. Accepted: 5 May 2021.

RESEARCH ARTICLE